Glioma Concentration Growth Simulation Using The Crank Nicolson Method

Viska Noviantri, Tomy Tjandra, Rinda Nariswari

***Abstract*—The most common type of central nervous system tumor in adults is glioma, accounting for about 70% of all brain tumors. Prediction of glioma growth became interesting to be analyzed to measure how severe the glioma is, plan the proper treatment, and estimate how long the patient can survive. This paper uses the Reaction-diffusion equation to interpret the glioma concentration in the grey and white matter of the brain based on three different growth functions. These are exponential, logistic, and Gompertzian growth functions. The Crank-Nicolson scheme is applied here to solve this model as an initial step to carry out the simulation. It is used since this scheme is unconditionally stable and has a higher order of accuracy. This scheme produces a linear system equation for exponential growth function while a nonlinear system for logistic and Gompertzian growth function. The simulation results include concentration, maximum concentration, cell number, and average speed of glioma cells for each growth function given here. As a result, the maximum glioma concentration grows infinitely for exponential growth but converges to specific values for logistic and Gompertzian growth functions. Furthermore, this paper gives the sensitivity analysis for the model to see the behavior of glioma concentration based on parameter changes. These are initial glioma position, net proliferation rate, and diffusivity coefficient in grey and white matter. It shows that net proliferation affects glioma concentration growth more than others.**

***Index Terms*—glioma, logistic, Gompertzian, reaction-diffusion, crank nicholson.**

I. Introduction

Brain tumors are abnormal cell growths around the brain. Like other tumors, brain tumors can be malignant (cancerous) or not. Brain tumors are rare because they accounted for 1.6% of cancer incidence, [1] and [2]. However, it has some risk factors if they grow to press on the nerves, blood vessels, and surrounding tissue [3]. The estimated survival rate for a person with a brain tumor is five years to 35% for malignant tumors and about 90% for benign tumors [4], [5].

Glioma is a type of brain tumor that develops from cells that would otherwise be solid glial cells, which support the central nervous system (CNS), in the brain [6], [7]. Many studies report that glioma is the most common type of CNS tumor in adults, accounting for about 70% of all brain tumors, [8], [9], [10], [11]. Therefore, many researchers study glioma with various approaches to get more information to find appropriate solutions to minimize glioma growth or treat it.

Several studies were conducted to provide information about factors that can increase the risk of glioma so that people can avoid it. Bielecka [12] and Ebrahimpour-Koujan [13] study about the nutritional and lifestyle effects on glioma incidence. Moreover, Zhang [14] and Bansal [15] not only analyze the impact of lifestyle but also dietary on glioma. They found that people with stress and a lack of exercise have a higher risk of developing a brain tumor. Regarding dietary intake of tea, it can reduce the glioma risk significantly. Green and orange vegetables may help to reduce the risk of glioma. While the intake of grains, processed meats, and fish may increase the risk of glioma.

The study of how to detect glioma continues not only by medical science but also by computer science approach [16], [17], [18]. Peddinti [19] reviews some developments in MRI processing as the first diagnosis and detection of brain tumors for segmentation and representation so that we can apply new machine learning methods (ML) in decision-making. Khan [20] use two deep learning model by a convolutional neural network (CNN) to detect brain tumor. These are "Proposed 23-layer CNN" and "Fine-tuned CNN with VGG16". The results show that the model has 97.8% and 100% prediction accuracy, respectively.

Research on gliomas not only how to detect but also how to predict glioma growth. Prediction of glioma growth is needed to measure how severe the glioma is, plan the proper treatment, and estimate how long the patient can survive. In the statistical approach, Silva [21] uses time series forecasting while Liang [22] uses the Bayesian Inference for glioma growth prediction. Alfonso [23] reviewed that mathematical models are very useful in representing the dynamics of glioma growth. Reaction-diffusion model is a common mathematical model that represents glioma growth which can solve numerically by several numerical methods [24], [25], [26], [27], [28].

In this paper, the Reaction-diffusion model is used to interpret the glioma concentration on the brain as a function of position and time. The piecewise function for the diffusivity coefficient is used here since the diffusivity in grey and white matter is different. Moreover, analyze the glioma concentration based on three different glioma growth functions applied here. These are exponential, logistic, and Gompertzian growth functions. The Crank-Nicolson scheme is used here to solve this model numerically since this scheme is unconditionally stable and has a higher order of accuracy [29],[30]. The scheme which produces a linear equation system for exponential growth while a nonlinear system for logistic and Gompertzian growth function. The simulation results include concentration, maximum concentration, cell number, and average speed of glioma cells given

Manuscript received May 16, 2023; revised September 28, 2023.

Viska Noviantri is a lecturer in the Mathematics Department, School of Computer Science, Bina Nusantara University, Jakarta, Indonesia 11480 (Corresponding author to provide phone: +62 21 534 5830; e-mail: viskanoviantri@binus.ac.id).

Tomy Tjandra is a postgraduate student in Computer Science and Information Engineering (CSIE), National Taiwan University of Science and Technology, Taipei, Taiwan 106 (e-mail: tomytjandra@gmail.com).

Rinda Nariswari is a lecturer in the Statistics Department, School of Computer Science, Bina Nusantara University, Jakarta, Indonesia 11480 (e-mail: rinda.nariswari@binus.ac.id).

here. These results have been validated with the previous research and completed by any analysis to see the differences between each growth function. Furthermore, this paper gives the sensitivity analysis to see the effect of parameter changes, including initial glioma position, net proliferation rate, and diffusivity coefficient in white and grey matter. The simulation and analysis results of the model can be used as consideration to plan the optimal treatment.

II. Governing Equation

Under the assumption that glioma grows in one spatial direction only in plane geometry, this phenomenon can be interpreted by reaction-diffusion equation as follows:

$$\frac{\partial c}{\partial t} = \frac{\partial}{\partial x}\left(D(x)\frac{\partial c}{\partial x}\right) + r(c) \tag{1}$$

where $c(x,t)$ is a glioma concentration in position x and time t. Here $D(x)$ is a diffusivity coefficient, and $r(c)$ is a glioma growth as a function of glioma concentration.

In general, the brain divides into white and grey matter zones. Let the brain length is L ($0 \leq x \leq L$), then the human brain divides into three domains which are white ($L_1 \leq x \leq L_1 + L_2$) and grey matter zone ($0 \leq x \leq L_1, L_1 + L_2 \leq x \leq L$). Glioma cells grow faster in the white zone than in the grey zone [31], [32], [33]. Therefore, the diffusivity coefficient is represented by

$$D(x) = \begin{cases} D_g, x\epsilon[0, L_1] \\ D_w, x\epsilon[L_1, L_1 + L_2] \\ D_g, x\epsilon[L_1 + L_2, L] \end{cases} \tag{2}$$

where D_g and D_w are the diffusivity coefficients in grey and white matter zones, respectively.

There are many different types of population growth in the deterministic biological approach, which can represent glioma growth, [34], [35], [36]. This study adapts three kinds of glioma growth ($r(c)$), named exponential, logistic, and Gompertzian, which was written by

$$r(c) = \rho c \tag{3}$$

$$r(c) = \rho c\left(1 - \frac{c}{K}\right) \tag{4}$$

$$r(c) = -\rho c \ln\left(\frac{c}{e^{\frac{k}{d}}}\right) \tag{5}$$

where ρ is net proliferation rate, K is the glioma carrying capacity for logistic growth function, $e^{k/d}$ is the glioma carrying capacity for Gompertzian growth function with k is growth rate and d is density coefficient of the glioma.

Furthermore, a zero flux condition is applied here. It means that there is no diffusion process at the boundary, such that the boundary condition becomes

$$\frac{\partial c(0,t)}{\partial x} = 0 \tag{6}$$

$$\frac{\partial c(L,t)}{\partial x} = 0 \tag{7}$$

Consider to [37] and [38], the initial condition for glioma concentration represented by the Gaussian function:

$$c(x,0) = g(x) = \frac{1}{\varepsilon\sqrt{2\pi}} e^{-\frac{1}{2}\left(\frac{x-x_0}{\varepsilon}\right)^2}, x\epsilon[0, L] \tag{8}$$

where x_0 is an initial glioma position and ε is a standard deviation to represent the initial glioma spreading.

By using the first derivative for function (8), it can be shown that the extreme point happens when $x = x_0$. Next, the second derivative of this function is

$$g''(x) = \frac{1}{\varepsilon^3\sqrt{2\pi}} e^{-\frac{1}{2}\left(\frac{x-x_0}{\varepsilon}\right)^2}\left(1 - \left(\frac{x - x_0}{\varepsilon}\right)\right) \tag{9}$$

By (9), the gaussian function (8) has a maximum c_0 when $x = x_0$, that is

$$c_0 = g(x_0) = \frac{1}{\varepsilon\sqrt{2\pi}} \tag{10}$$

so that

$$\varepsilon = \frac{1}{c_0\sqrt{2\pi}} \tag{11}$$

Substitute (11) into (8) then the initial condition for the governing equation is

$$c(x,0) = c_0 e^{-\frac{1}{2}\left((x-x_0)\sqrt{2\pi}c_0\right)^2}, x\epsilon[0, L] \tag{12}$$

III. Crank Nicolson Method

The glioma growth observation domain is uniformly discretized so that the lengths of the x and t-axis are

$$\Delta x = x_{j+1} - x_j \tag{13}$$

$$\Delta t = t_{n+1} - t_n \tag{14}$$

with $j, n = 0, 1, 2, ...$ Obviously, the glioma concentration after discretization at point (j, n) represent as c_j^n.

The governing equation (1) will be solved by the Crank-Nicolson method so that the discrete scheme for this equation at the point $(j, n + \frac{1}{2})$ is

$$\left.\frac{\partial c}{\partial t}\right|_j^{n+\frac{1}{2}} = \frac{\partial}{\partial x}\left(D(x)\frac{\partial c}{\partial x}\right)\Bigg|_j^{n+\frac{1}{2}} + r\left(c_j^{n+\frac{1}{2}}\right) \tag{15}$$

Apply the forward difference scheme to approximate the first derivative over time t at point $(j, n + \frac{1}{2})$,

$$c_t|_j^{n+\frac{1}{2}} = \left.\frac{\partial c}{\partial t}\right|_j^{n+\frac{1}{2}} = \frac{c_j^{n+1} - c_j^n}{\Delta t} \tag{16}$$

and the average formula for glioma concentration at point $(j, n + \frac{1}{2})$ is

$$c|_j^{n+\frac{1}{2}} = \frac{c_j^{n+1} + c_j^n}{2} \tag{17}$$

Use (17) to rewrite the first term on the right-hand side equation (15), that is

$$\begin{aligned} &\tfrac{\partial}{\partial x}\left(D(x)\tfrac{\partial c}{\partial x}\right)\Big|_j^{n+\frac{1}{2}} \\ &= \tfrac{1}{2}\left[\tfrac{\partial}{\partial x}\left(D(x)c_x\right)\Big|_j^{n+1} + \tfrac{\partial}{\partial x}\left(D(x)c_x\right)\Big|_j^{n}\right] \end{aligned} \tag{18}$$

where the first derivative over spatial domain x at point (j, n) approximate by the center difference:

$$c_x|_j^n = \left.\frac{\partial c}{\partial x}\right|_j^n = \frac{c_{j+\frac{1}{2}}^n - c_{j-\frac{1}{2}}^n}{\Delta x} \tag{19}$$

Replace c in equation (19) by $D(x)c_x$ to get

$$\frac{\partial}{\partial x}\left(D(x)\frac{\partial c}{\partial x}\right)\Bigg|_j^n = \frac{D_{j+\frac{1}{2}}^n (c_x)_{j+\frac{1}{2}}^n - D_{j+\frac{1}{2}}^n (c_x)_{j-\frac{1}{2}}^n}{\Delta x} \tag{20}$$

Next, do some algebraic manipulation for equation (18)-(20) to get the simplest form of the first term on the right-hand side equation (15). Substitute this form, together with (16) and (19), into equation (15) so that the Crank Nicolson scheme for the problem becomes

$$\begin{aligned}&\frac{c_j^{n+1}-c_j^n}{\Delta t} = \\ &\frac{1}{2(\Delta x)^2}\left[D_{j+\frac{1}{2}}^{n+1}c_{j+1}^{n+1} - \left(D_{j+\frac{1}{2}}^{n+1}+D_{j-\frac{1}{2}}^{n+1}\right)c_j^{n+1} + D_{j-\frac{1}{2}}^{n+1}c_{j-1}^{n+1}\right. \\ &\left.+D_{j+\frac{1}{2}}^{n}c_{j+1}^{n} - \left(D_{j+\frac{1}{2}}^{n}+D_{j-\frac{1}{2}}^{n}\right)c_j^{n} + D_{j-\frac{1}{2}}^{n}c_{j-1}^{n}\right] \\ &+\frac{r}{2}\left[c_j^{n+1}+c_j^n\right]\end{aligned} \tag{21}$$

with

$$D_{j+\frac{1}{2}}^n = D\left(\left(j+\frac{1}{2}\right)\Delta x\right)$$

$$D_{j-\frac{1}{2}}^n = D\left(\left(j-\frac{1}{2}\right)\Delta x\right)$$

The Neumann boundary condition (6) and (7) approximated by center difference as follows

$$\frac{c_2^{n+1}-c_0^{n+1}}{2\Delta x} = 0 \tag{22}$$

$$\frac{c_p^{n+1}-c_{p-2}^{n+1}}{2\Delta x} = 0 \tag{23}$$

where p is a spatial grid number and the initial condition (12) become

$$c_j^0 = c_0 e^{-\frac{1}{2}((j\Delta x - x_0)\sqrt{2\pi}c_0)^2} \tag{24}$$

Furthermore, the numerical method (21) for each growth function (3)-(5) is explained in the following subsection.

A. Exponential Growth

The numerical scheme (21) with growth function (3) give the following scheme

$$\begin{aligned}&Wc_{j-1}^{n+1} + (1+V)c_j^{n+1} + Uc_{j+1}^{n+1} \\ &= -Wc_{j-1}^n + (1-V)c_j^n + Uc_{j+1}^n\end{aligned} \tag{25}$$

where

$$U = -RD_{j+\frac{1}{2}} \tag{26}$$

$$V = -S + R\left(D_{j+\frac{1}{2}} + D_{j-\frac{1}{2}}\right) \tag{27}$$

$$W = -RD_{j-\frac{1}{2}} \tag{28}$$

$$R = \frac{\Delta t}{2(\Delta x)^2} \tag{29}$$

$$S = \frac{\rho \Delta t}{2} \tag{30}$$

Iterate equation (25) from $j = 1$ to $j = P-1$, to produce the following linear equation system

$$A\overrightarrow{c}^{n+1} = B\overrightarrow{c}^n \tag{31}$$

where

$$\overrightarrow{c}^n = \left(c_1^n c_2^n ... c_{p-1}^n\right)^T \tag{32}$$

$$\overrightarrow{c}^{n+1} = \left(c_1^{n+1} c_2^{n+1} ... c_{p-1}^{n+1}\right)^T \tag{33}$$

Furthermore, $A = \alpha + \gamma$ and $B = \beta - \gamma$ are a matrix with size $(P-1 \times P-1)$ with entry:

$$\alpha_{b,i} = \begin{cases} W, & i = b-1 \\ 1+V, & i = b \\ U, & i = b+1 \\ 0, & otherwise \end{cases} \tag{34}$$

$$\beta_{b,i} = \begin{cases} -W, & i = b-1 \\ 1-V, & i = b \\ -U, & i = b+1 \\ 0, & otherwise \end{cases} \tag{35}$$

$$\gamma_{b,k} = \begin{cases} U, & b = P-1 and i = P-2 \\ W, & b = 1 and i = 2 \\ 0, & otherwise \end{cases} \tag{36}$$

B. Logistic Growth

The numerical scheme (21) with growth function (4) give the following scheme

$$\begin{aligned}&T(c_j^{n+1}+c_j^n)^2 + Uc_{j+1}^{n+1} + (V+1)c_j^{n+1} \\ &+Wc_{j-1}^{n+1} + Uc_{j+1}^n + (V-1)c_j^n + Wc_{j-1}^n = 0\end{aligned} \tag{37}$$

where U, V, and W as in (26)-(28) and

$$T = \frac{\rho \Delta t}{4K}$$

This nonlinear equation system (37) solved for c^{n+1} by Newton Rapshon Method with stopping criteria as follows

$$\|\overrightarrow{\Delta c}\| \leq \varepsilon_r \|\overrightarrow{c_0}^{n+1}\| + \varepsilon_a \tag{38}$$

where $\|\cdot\|$ is Euclidean norm, ε_r and ε_a are relative and absolute error, respectivelly.

C. Gompertzian Growth

The numerical scheme (21) with growth function (5) give the following scheme

$$\begin{aligned}&S(c_j^{n+1}+c_j^n)\ln\left(\frac{c_j^{n+1}+c_j^n}{2}\right) \\ &+Wc_{j-1}^{n+1} + Uc_{j+1}^{n+1} + (Z+1)c_j^{n+1} \\ &+Wc_{j-1}^n + Uc_{j+1}^n + (Z-1)c_j^n \quad = \quad 0\end{aligned} \tag{39}$$

where U, W, and S as in (26), (28) and (30), then

$$Z = \frac{k\rho\Delta t}{2d} + R\left(D_{j+\frac{1}{2}} + D_{j-\frac{1}{2}}\right)$$

As in Logistic Growth, the nonlinear system (39) is solved by Newton Raphson method with the same stopping criteria.

IV. Glioma Cell Atribute

The glioma concentration $c(x,t)$ can be used to calculate some glioma cell attributes: Maximum concentration ($c_{max}(t)$), total cell number ($N(t)$), total mean radial distance ($L(t)$) and average speed of glioma cells ($S(t)$) over time t which represented by

$$c_{max}(t) = max(c(x,t)), 0 \leq x \leq L, \tag{40}$$

$$N(t) = \int_Z^L c(x,t)dx, \tag{41}$$

TABLE I
PARAMETER INPUT

Parameter	Value	Unit	Refference
L_1	7.5	mm	[24]
L_2	35	mm	[24]
L	50	mm	[24]
D_g	0.13	mm^2/day	[24]
D_w	0.65	mm^2/day	[24]
x_0	25	mm	[24]
ρ	0.012	/day	[24]
ε	0.01	cell/mm	[24]
K	62.5	cell/mm	[24]
k/d	4.135	cell/mm	[26]
Δx	0.5	mm	[26]
Δt	1	day	[26]
ε_a	10^{-5}		[26]
ε_r	10^{-5}		[26]

$$L(t) = \frac{1}{N(t)} \int_0^L xc(x,t)dx, \tag{42}$$

$$S(t) = \frac{dL(t)}{dt}. \tag{43}$$

The maximum concentration (40) is approximated directly by using the following discretization,

$$c^n_{max} = max\{c^n_j\}, \tag{44}$$

whereas the total cell number (41) and total mean radial (42) distance solved by Simpson 1/3 rules as follows

$$N^n = \frac{\Delta x}{3}\left[c^n_a + \sum_{j\in odd} 4c^n_j + \sum_{j\in even} 2c^n_j + c^n_b\right], \tag{45}$$

$$L^n = \frac{(\Delta x)^2}{3N^n}\left[ac^n_a + \sum_{j\in odd} 4jc^n_j + \sum_{j\in even} 2jc^n_j + bc^n_b\right], \tag{46}$$

where a and b are the first and the last index in spatial domain discretization.

The center finite difference is applied to approximate the average speed of glioma cells (43) numerically as

$$S^n = \frac{L^{n+1} - L^{n-1}}{2\Delta t}. \tag{47}$$

V. SIMULATION RESULTS

This section shows simulation results to analyze the glioma concentration and some of their attributes based on different growths. For this purpose, the simulation is conducted by parameter input, as shown in Table I. Note that the initial condition of glioma concentration is represented by (8) with x_0 and ε as in Table I.

Figure 1 represents the glioma concentration over time and spatial domain with logistic growth function. It shows that the concentration at time $t = 0$ means the Gaussian function (8) with the maximum concentration $c_{0max} = 39.89$ cells/mm as the analytical solution (10). When $t = 0.076$, the maximum glioma concentration becomes 4.344 cells/mm. It means that the glioma concentration drops about 35 cells/mm in 0.076 days only. In addition, Figure 2 shows that glioma concentration decreases quickly from day 0 until day 25.

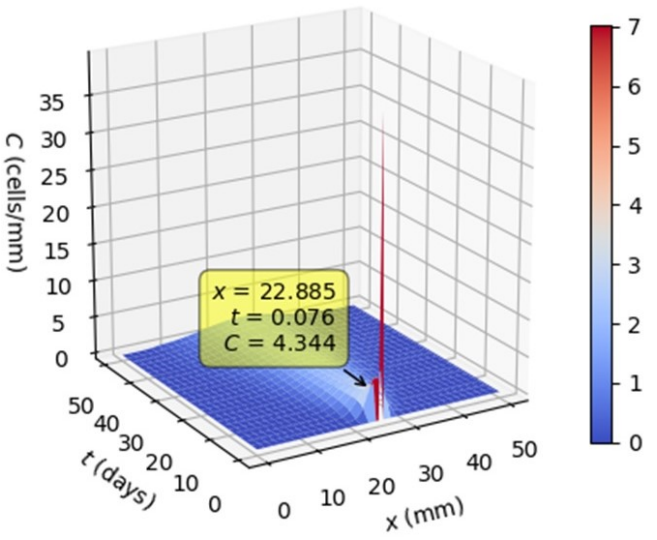

Fig. 1. The Glioma Concentration for Logistic Growth in Three-Dimensional Axis

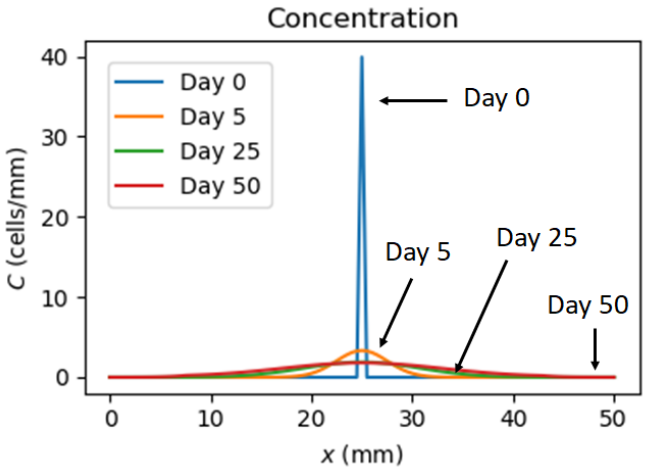

Fig. 2. The Glioma Concentration for Logistic Growth at time $t \leq 50$ days

However, the concentration at time $t == 25$ days (green curve) is less than at time $t = 50$ days (red curve). This result suggests that the situation reverses at a specific time. It occurs at time $t = 42$ days.

For further analysis, the simulation was carried out more than 42 days. Figure 3 - 5 shows the glioma concentration as a function of spatial direction for exponential, logistic, and Gompertzian growth functions at three different times, respectively. In each figure, blue, green, and red lines show the concentration in time $t = 100, 150$, and 200 days. It shows that the glioma concentration increases as a function of time when $t \geq 100$. It is contradictive with $t < 42$ days as in Figure 1. These figures also represented the diffusivity coefficient's effect on glioma concentration. Since $D_w \geq D_g$ as in Table I, the glioma spread faster in white matter ($7.5 \leq x \leq 42.5$) than in the grey matter ($x \leq 7.5$ or $x \geq 42.5$). At these three times, the biggest glioma concentration occurs in the Gompertzian growth function, followed by logistic and exponential growth functions. In Gompertzian, the maximum glioma concentration at time $t = 200$ days up to 38 cells/mm, whereas the concentration in logistic and exponential is only

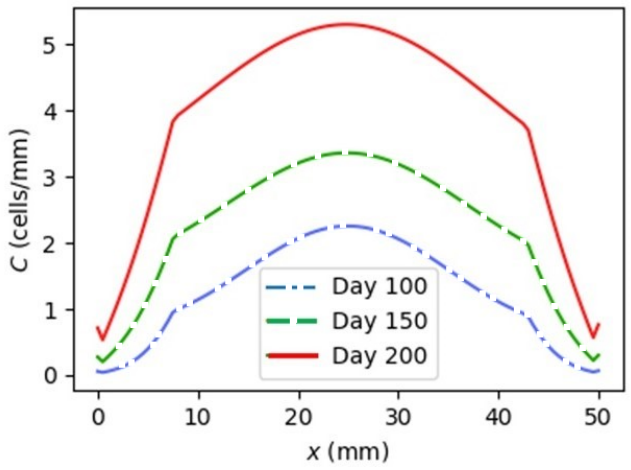

Fig. 3. The Glioma Concentration for Exponential Growth Function

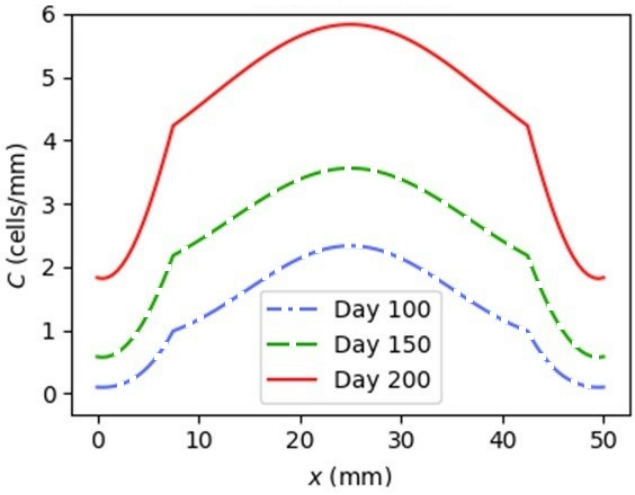

Fig. 4. The Glioma Concentration for Logistic Growth Function

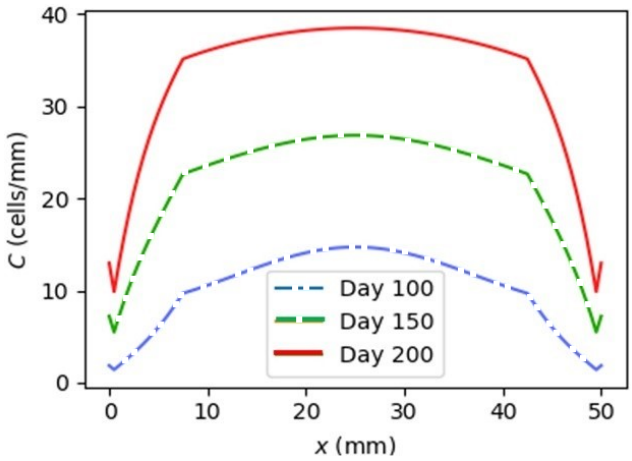

Fig. 5. The Glioma Concentration for Gompertzian Growth Function

about 6 and 5 cells/mm, respectively.

The maximum value of glioma concentration from all spatial axes can be derived for more analysis through (44) and shown in Figure 6 and 7. In Figure 6, the maximum glioma concentration for exponential growth increases slightly for time $t \leq 1000$ days, then increases significantly afterward. It never goes to some constant since the exponential function is not bounded by carrying capacity. Meanwhile, as in Figure

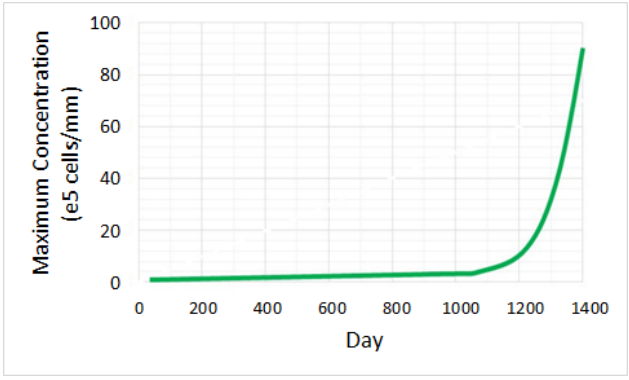

Fig. 6. Maximum Glioma Concentration by Exponential Growth Function

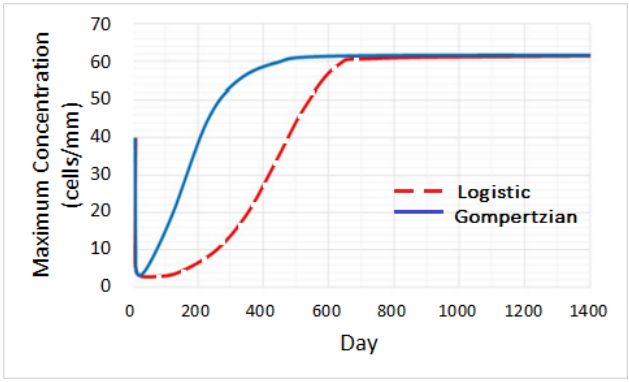

Fig. 7. Maximum Glioma Concentration by Logistic (red) and Gompertzian (blue) Growth Function

7, the maximum glioma concentration for Logistic growth (a red curve) and Gompertzian growth (a blue curve) will drop quickly for time $t \leq 42$ days. After that, the maximum value increases significantly in the domain $42 \leq t \leq 700$ days for logistic growth and $42 \leq t \leq 500$ days for Gompertzian growth, then goes to constant. It means that the maximum glioma concentration for Gompertzian growth reaches the equilibrium point faster than logistic growth. The equilibrium point is 62.5 cells/mm, satisfying the glioma carrying capacity as in Table I. Furthermore, it can be seen that the maximum concentration in the domain $42 \leq t \leq 500$ begins from the greatest to the smallest in Gompertzian, logistic, and exponential growth functions, which are in line with the previous simulations. Overall, the simulation results for logistic growth related to Viska [26] and Ozugurlu [24].

After approximating the cell number (45) numerically, the glioma attribute over time for each zone can be obtained. Let zone 1 for $x \in [0, L_1]$, zone 2 for $x \in [L_1, L_1 + L_2]$, and zone 3 for $x \in [L_1 + L_2, L]$. The cell number over time for each zone is described in Figure 8 - 10. The cell number in the grey zone, zone 1 and zone 3 is always smaller than in the white zone (zone 2), following the diffusivity coefficient in their zones. It can be seen that the cell numbers follow the glioma concentration pattern, where the exponential function leads to infinite growth. In contrast, the cell number for logistic and Gompertzian growth convergent to $N = 2000$ cells in the white zone and $N = 600$ cells in the grey zone. However, Gompertzian is faster than the logistic growth function to reach the equilibrium point.

Next, substitute (46) into (47) to get the average speed of glioma cells over time for each zone, as shown in Figure

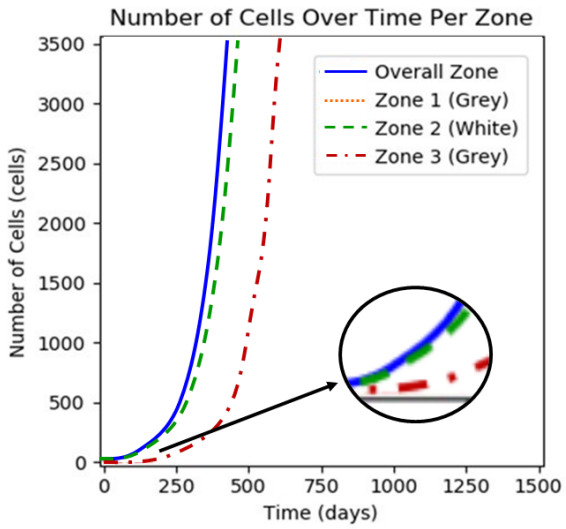

Fig. 8. The Glioma Cell Number for Exponential Growth Function

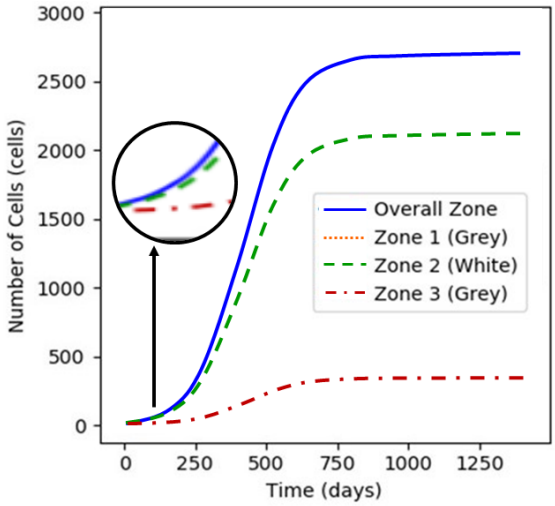

Fig. 9. The Glioma Cell Number for Logistic Growth Function

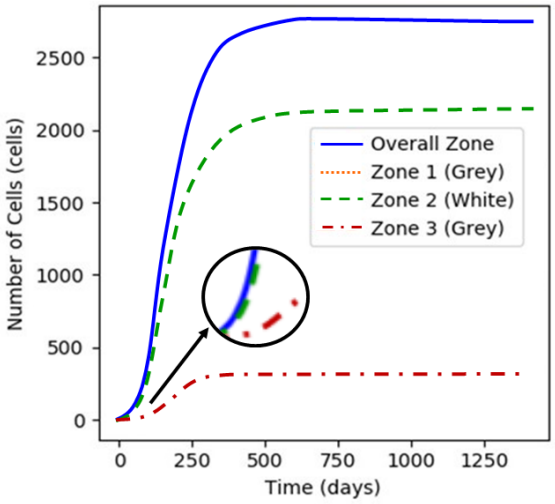

Fig. 10. The Glioma Cell Number for Gompertzian Growth Function

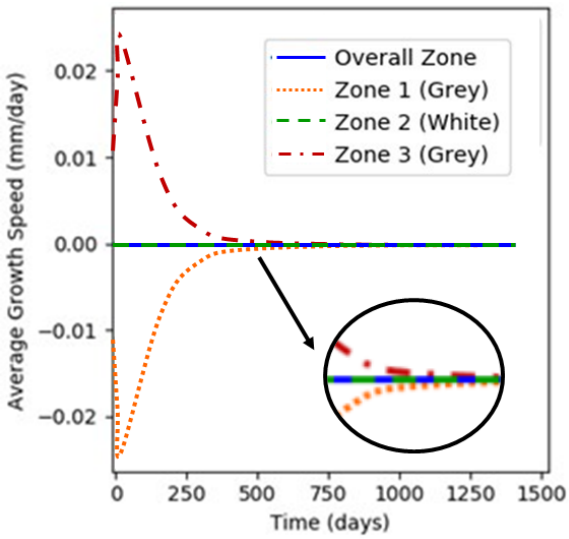

Fig. 11. The Average Speed of Glioma Growth for Exponential Growth

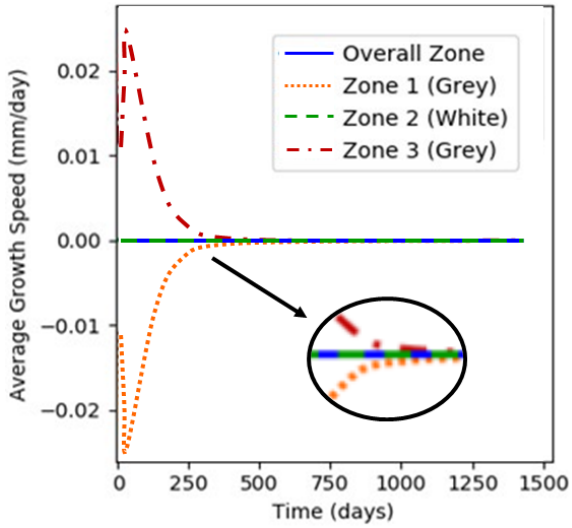

Fig. 12. The Average Speed of Glioma Growth for Logistic Growth

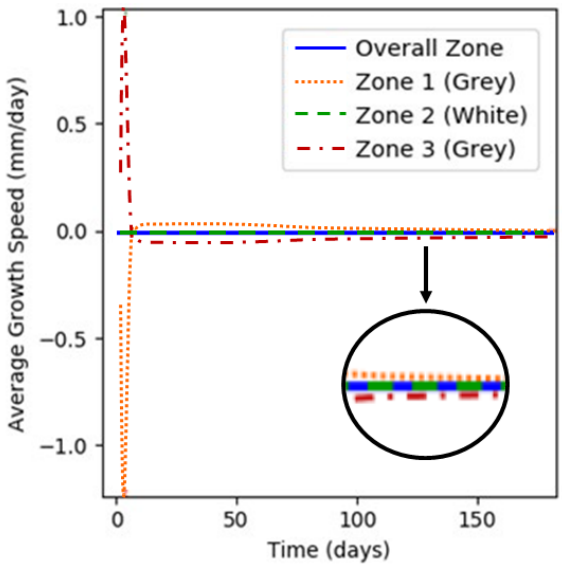

Fig. 13. The Average Speed of Glioma Growth for Gompertzian Growth

11-13. The glioma growth speed changes drastically only in the initial phase, from $t = 0$ to $t \approx 250$ for exponential and logistic function, from $t = 0$ to $t \approx 20$ for Gompertzian

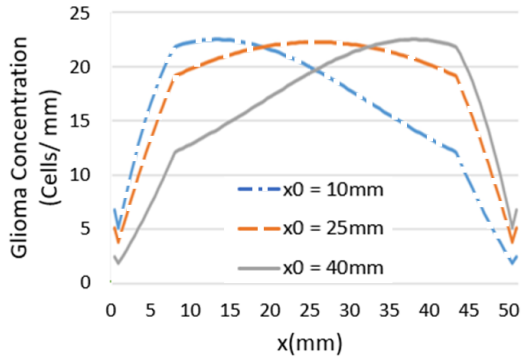

Fig. 14. The Glioma Concentration in Different Initial Positions (x_0)

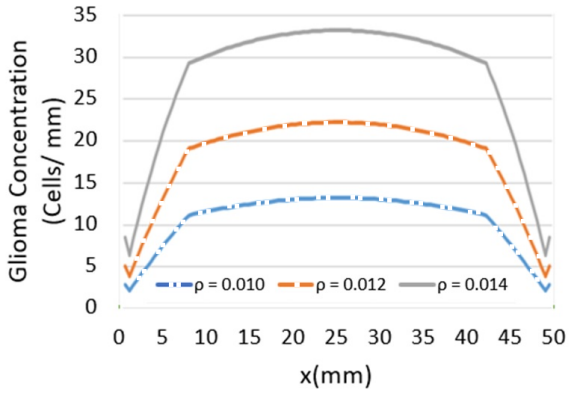

Fig. 15. The Glioma Concentration in Different Proliferation Rate (ρ)

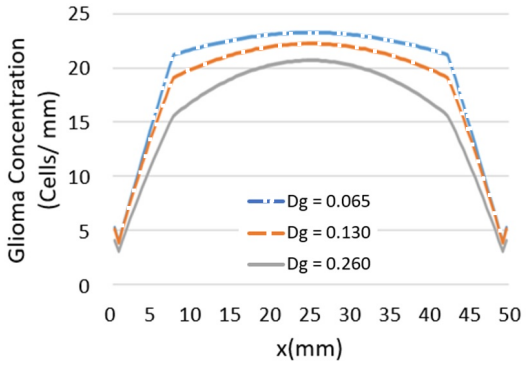

Fig. 16. The Glioma Concentration in Different Diffusivity Coefficients in Grey Matter Zones D_g

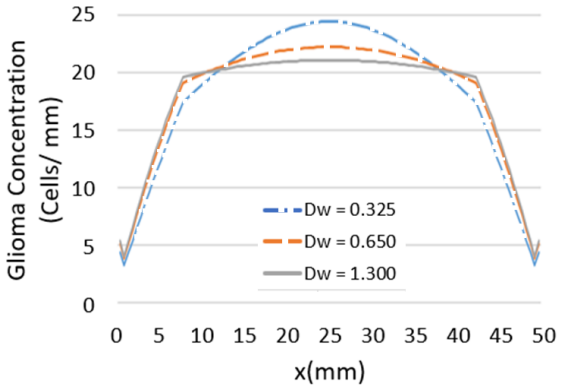

Fig. 17. The Glioma Concentration in Different Diffusivity Coefficients in White Matter Zones D_w

function. After that, the growth speed remains relatively constant for all zones. These figures also show that the average speed in Zone 1 is negative since the initial glioma is in Zone 2 so the radial distance grows to the left domain ($x < L_1$). In contrast, the average speed in Zone 3 is positive because the radial distance grows to the right domain ($x > L_1 + L_2$). The Gompertzian growth has the highest speed since the speed is up to $|1|$ mm/day. Meanwhile, the exponential and logistic growth is only up to 0.025 mm/day. Nevertheless, these figures show that the average speed in Gompertzian is up and down quickly at times less than 20 days and goes to 0 afterward. In contrast, logistic and exponential need 500 and 750 days to converge to 0. Based on these simulation results, the Gompertzian growth will describe the glioma growth much better than the others.

VI. Sensitivity Analysis for Gompertzian Growth Function

Vaghi [35] and Akin [39] stated that the Gompertzian growth function describes tumor growth better than the other by an experimental approach. Here, the Gompertzian growth function gives the same results since it has become the fastest growth of glioma concentration. Sensitivity analysis is conducted here to see the effect of changes in one of the parameters on the output results. In this section, sensitivity analysis for the glioma concentration by the Gompertzian growth function is carried out by four parameters. These are initial glioma position (x_0), net proliferation rate (ρ), and diffusivity coefficient in grey and white matter (D_g and D_w).

Figure 14 - 17 describes the parameter sensitivity for the glioma concentration at time $t = 365$ days and range $1 \leq x \leq 50$. In addition, Figure 18 - 21 illustrates the parameter sensitivity for the maximum glioma concentration over time. Each figure consists of three different values of one parameter. In contrast, the other parameters are fixed as in Table I.

In Figure 14, the maximum glioma concentration occurs at the initial glioma position, related to the basic medical concept. At the time $t = 365$ days, When the initial position $x_0 = 10$ mm and 40 mm, then the maximum concentration is 22.4896 cells/mm, but the maximum concentration becomes 22.2438 cells/mm when the initial position $x_0 = 25$. By Figure 18, the maximum concentration is bigger when the initial position of the glioma is in the grey matter zone (x_0 = 10 and 40 mm) for $t \leq 381$ days, then switches after that time.

The effect of net proliferation rate (ρ) is shown in Figure 15 and 19, where a blue, an orange, and a grey line for $\rho = 0.010; 0.012;$ and 0.014, respectively. The greater proliferation rate leads to greater glioma concentration. Furthermore, the maximum glioma concentration at time $t = 365$ days when $\rho = 0.010; 0.012;$ and 0.014 are $14, 22$ and 34 cell/mm, which means that the glioma concentration increases up to 50% even though the proliferation rate increases only about 20%. Figure 19 also shows that the bigger net proliferation rate makes the glioma concentration reach the equilibrium point faster.

The diffusivity coefficient in grey and white matter gives different results as in Figure 16, 17, 20, and 21. As in Figure 16, a bigger diffusivity coefficient in grey matter (D_g)

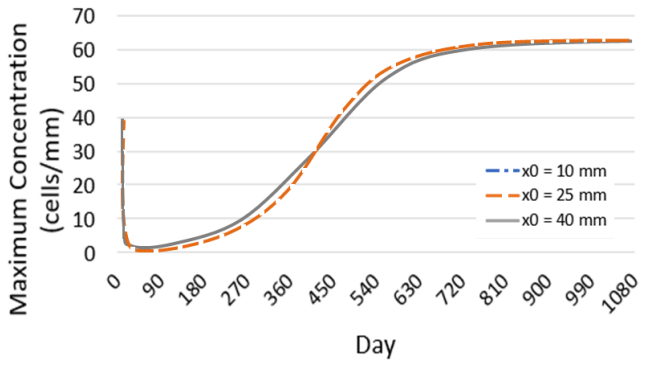

Fig. 18. The Maximum Glioma Concentration in Different Initial Positions (x_0)

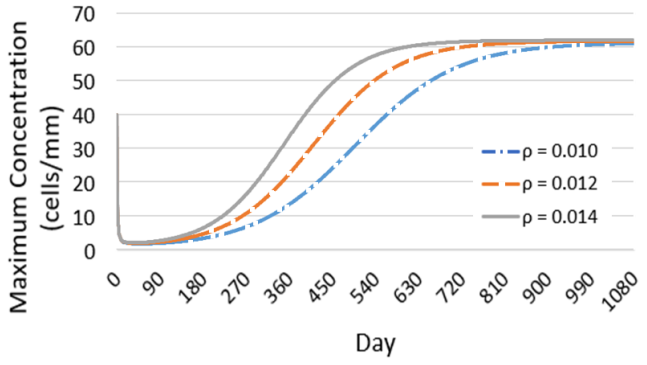

Fig. 19. The Glioma Concentration in Different Proliferation Rate (ρ)

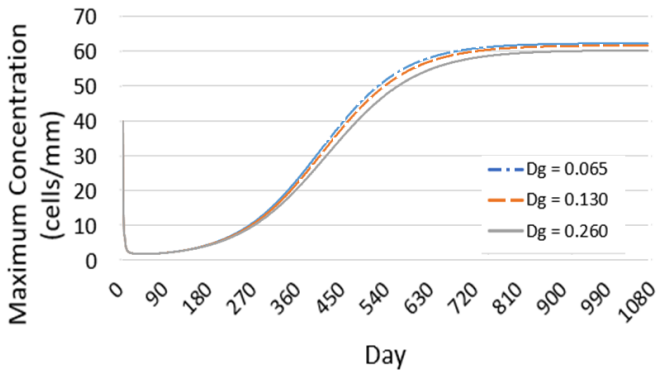

Fig. 20. The Maximum Glioma Concentration in Different Diffusivity Coefficients in Grey Matter Zones D_g

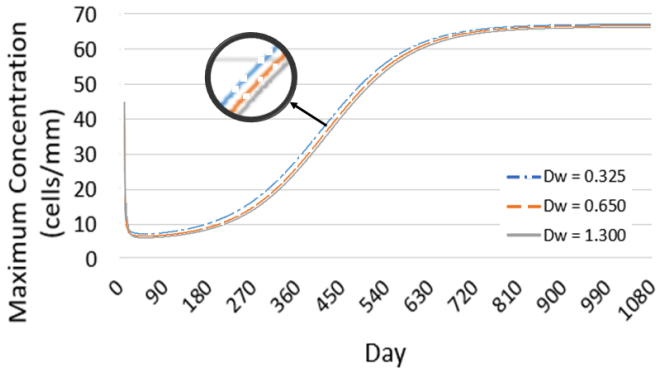

Fig. 21. The Maximum Glioma Concentration in Different Diffusivity Coefficients in White Matter Zones D_w

leads to a smaller glioma concentration at any position. This condition does not occur in the changes of the diffusivity coefficient in white matter (D_w). Figure 17 shows that the glioma concentration graph split at some position. Around the white matter area (in the middle of the axis), a bigger diffusivity coefficient in white matter (D_w) leads to a smaller glioma concentration at any position. The opposite condition occurs around the grey matter area. The glioma concentration changes slightly (less than 10%) even though the diffusivity coefficient varies twice in grey and white matter. The diffusivity coefficient does not significantly affect the maximum glioma concentration, as shown in Figure 20 and 21. Based on these sensitivity analyses, we conclude that the net proliferation rate significantly affects the glioma concentration more than the other parameters.

VII. Conclusion

The reaction-diffusion model, solved by the Crank-Nicolson scheme, has successfully represented the glioma concentration growth with different diffusivity coefficients for each matter zone. The simulation results show that the exponential growth function produces glioma growth patterns very different from the logistic and Gompertzian growth functions. By the exponential growth function, glioma concentration increased unlimited, which is related to the analytical analysis. The logistics and Gompertzian show that the glioma decreases quickly at the starting period and then increases, converging to their carrying capacity value. The glioma cell number shows the same pattern as their concentration since the cell number is proportional to its concentration.

Furthermore, the Gompertzian growth function describes the glioma growth better since it has the highest average speed growth and significantly differs from the others. This result is related to [35] and Akin [39]. The sensitivity analysis indicates that different diffusivity coefficients for each matter zone influence the glioma concentration growth in each zone since this parameter describes the ability of the cell to diffuse across the unit area. Moreover, the net proliferation rate significantly affects the concentration and the total number of glioma cells more than the other parameters. It means that the ability of glioma cells to copy their DNA plays an essential role in the glioma growth model.

References

[1] T. Aninditha, P. Pratama, H. Sofyan, D. Imran, R. Estiasari, F. Octaviana, M. Iskandar, J. Odilo, R. Werdhani, R. Aman, and T. Ranakusuma, "Adults brain tumor in cipto mangunkusumo general hospital: A descriptive epidemiology," *Romanian Journal of Neurology*, vol. 20, no. 4, pp. 480–484, 2021.

[2] H. Sung, J. Ferlay, R. L. Siegel, M. Laversanne, I. Soerjomataram, A. Jemal, and F. Bray, "Global cancer statistics 2020: Globocan estimates of incidence and mortality worldwide for 36 cancers in 185 countries," *CA: A Cancer Journal for Clinicians*, vol. 71, no. 3, pp. 209–249, 2021. [Online]. Available: https://acsjournals.onlinelibrary.wiley.com/doi/abs/10.3322/caac.21660

[3] M. Pichaivel, G. Anbumani, P. Theivendren, and M. Gopal, *An Overview of Brain Tumor*, 2022.

[4] A. Neugut, P. Sackstein, G. Clarke Hillyer, J. Jacobson, J. Bruce, A. Lassman, and P. Stieg, "Magnetic resonance imaging-based screening for asymptomatic brain tumors: A review," *The Oncologist*, vol. 24, no. 3, p. 375–384, 2019. [Online]. Available: https://doi.org/10.1634/theoncologist.2018-0177

[5] K. A. AA, S. Amina, A. Muhammad, A. Hina, K. O. T, A. O. O, and O. S. O, "Brain tumor: An overview of the basic clinical manifestations and treatment," *Global Journal of Cancer Therapy*, pp. 038–041, 2020. [Online]. Available: https://doi.org/10.17352/2F2581-5407.000034

[6] T. Oishi, S. Koizumi, and K. Kurozumi, "Molecular mechanisms and clinical challenges of glioma invasion," *Brain Sciences*, vol. 12, no. 2, 2022. [Online]. Available: https://www.mdpi.com/2076-3425/12/2/291

[7] Dr.R.Manivannan, Dr.S.Kameshwaran, V.Srividhya, P.Thirumurugan, and R.Gokul, "A comprehensive review on glioma," *International Journal of Allied Medical Sciences and Clinical Research*, vol. 9, no. 2, pp. 131–134, 2021. [Online]. Available: https://ijamscr.com/ijamscr/article/view/985

[8] Y. Fan, X. Zhang, C. Gao, S. Jiang, H. Wu, Z. Liu, and T. Dou, "Burden and trends of brain and central nervous system cancer from 1990 to 2019 at the global, regional, and country levels," *Archives of Public Health*, vol. 80, 2022. [Online]. Available: https://doi.org/10.1186/s13690-022-00965-5

[9] A. Patel, J. Fisher, E. Nichols, F. Abd-Allah, J. Ebro, A. Abdelalim, H. Niguse, D. Agius, F. Alahdab, T. Alam, C. Allen, N. Anber, A. Awasthi, H. Badali, A. Belachew, A. Bijani, T. Bjørge, F. Carvalho, F. Catalá-López, and A. Samy, "Global, regional, and national burden of brain and other cns cancer, 1990-2016: A systematic analysis for the global burden of disease study 2016," *The Lancet Neurology*, vol. 18, no. 4, pp. 376–393, 2019. [Online]. Available: https://doi.org/10.1016/S1474-4422(18)30468-X

[10] K. M. Walsh, H. Ohgaki, and M. R. Wrensch, "Chapter 1 - epidemiology," in *Gliomas*, ser. Handbook of Clinical Neurology, M. S. Berger and M. Weller, Eds. Elsevier, 2016, vol. 134, pp. 3–18. [Online]. Available: https://doi.org/10.1016/B978-0-12-802997-8.00001-3

[11] D. Lin, M. Wang, Y. Chen, J. Gong, L. Chen, X. Shi, F. Lan, Z. Chen, T. Xiong, H. Sun, and S. Wan, "Trends in intracranial glioma incidence and mortality in the united states, 1975-2018," *Frontiers in Oncology*, vol. 11, 2021. [Online]. Available: https://www.frontiersin.org/articles/10.3389/fonc.2021.748061

[12] J. Bielecka and R. Markiewicz-Żukowska, "The influence of nutritional and lifestyle factors on glioma incidence," *Nutrients*, vol. 12, no. 6, 2020. [Online]. Available: https://www.mdpi.com/2072-6643/12/6/1812

[13] S. Ebrahimpour-Koujan, M. Shayanfar, M. Mohammad-Shirazi, G. Sharifi, and A. Esmaillzadeh, "A Combined Healthy Lifestyle Score in Relation to Glioma: A Case-Control Study," *Current Developments in Nutrition*, vol. 5, p. 267, 2021. [Online]. Available: https://www.sciencedirect.com/science/article/pii/S2475299123107852

[14] W. Zhang, J. Jiang, X. Li, Y. He, F. Chen, and W. Li, "Dietary factors and risk of glioma in adults: A systematic review and dose-response meta-analysis of observational studies," *Frontiers in Nutrition*, vol. 9, 2022.

[15] N. Bansal, P. Dawande, S. Shukla, and S. Acharya, "Effect of lifestyle and dietary factors in the development of brain tumors," *Journal of Family Medicine and Primary Care*, vol. 9, no. 10, pp. 5200–5204, 2020.

[16] P. G. Brindha, M. Kavinraj, P. Manivasakam, and P. Prasanth, "Brain tumor detection from mri images using deep learning techniques," *IOP Conference Series: Materials Science and Engineering*, vol. 1055, no. 1, p. 012115, 2021. [Online]. Available: https://dx.doi.org/10.1088/1757-899X/1055/1/012115

[17] S. Merkaj, R. C. Bahar, T. Zeevi, M. Lin, I. Ikuta, K. Bousabarah, G. I. Cassinelli Petersen, L. Staib, S. Payabvash, J. T. Mongan, S. Cha, and M. S. Aboian, "Machine learning tools for image-based glioma grading and the quality of their reporting: Challenges and opportunities," *Cancers*, vol. 14, no. 11, 2022. [Online]. Available: https://www.mdpi.com/2072-6694/14/11/2623

[18] J. Amin, M. Sharif, A. Haldorai, M. Yasmin, and R. S. Nayak, "Brain tumor detection and classification using machine learning: a comprehensive survey," *Complex & Intelligent Systems*, vol. 8, pp. 3161 – 3183, 2022.

[19] A. S. Peddinti, S. Maloji, and K. Manepalli, "Evolution in diagnosis and detection of brain tumor – review," *Journal of Physics: Conference Series*, vol. 2115, no. 1, p. 012039, 2021. [Online]. Available: https://dx.doi.org/10.1088/1742-6596/2115/1/012039

[20] M. S. I. Khan, A. Rahman, T. Debnath, M. R. Karim, M. K. Nasir, S. S. Band, A. Mosavi, and I. Dehzangi, "Accurate brain tumor detection using deep convolutional neural network," *Computational and Structural Biotechnology Journal*, vol. 20, pp. 4733–4745, 2022. [Online]. Available: https://www.sciencedirect.com/science/article/pii/S2001037022003737

[21] L. Silva, G. Alvarez, E. Christo, G. Pelén Sierra, and V. Garcia, "Time series forecasting using arima for modeling of glioma growth in response to radiotherapy," *Semina: Ciências Exatas e Tecnológicas*, vol. 42, no. 1, pp. 3–12, 2021. [Online]. Available: https://doi.org/10.5433/1679-0375.2021v42n1p3

[22] B. Liang, J. Tan, L. Lozenski, D. A. Hormuth II, T. E. Yankeelov, U. Villa, and D. Faghihi, "Bayesian inference of tissue heterogeneity for individualized prediction of glioma growth," *IEEE Transactions on Medical Imaging*, pp. 1–1, 2023.

[23] J. Alfonso, K. Talkenberger, M. Seifert, B. Klink, A. Hawkins-Daarud, K. Swanson, H. Hatzikirou, and A. Deutsch, "The biology and mathematical modelling of glioma invasion: A review," *Journal of The Royal Society Interface*, vol. 14, p. 20170490, 2017.

[24] E. Özuğurlu, "A note on the numerical approach for the reaction–diffusion problem to model the density of the tumor growth dynamics," *Computers and Mathematics with Applications*, vol. 69, no. 12, pp. 1504–1517, 2015. [Online]. Available: https://www.sciencedirect.com/science/article/pii/S0898122115001996

[25] D. A. Hormuth, S. L. Eldridge, J. A. Weis, M. I. Miga, and T. E. Yankeelov, *Mechanically Coupled Reaction-Diffusion Model to Predict Glioma Growth: Methodological Details*. New York, NY: Springer New York, 2018, pp. 225–241. [Online]. Available: https://doi.org/10.1007/978-1-4939-7493-111

[26] V. Noviantri, T. Tomy, and A. Chowanda, "Linear and nonlinear model of brain tumor growth simulation using finite difference method," *Procedia Computer Science*, vol. 179, pp. 297–304, 2021, 5th International Conference on Computer Science and Computational Intelligence 2020. [Online]. Available: https://www.sciencedirect.com/science/article/pii/S1877050921000107

[27] C. Martens, A. Rovai, D. Bonatto, T. Metens, O. Debeir, C. Decaestecker, S. Goldman, and G. Van Simaeys, "Deep learning for reaction-diffusion glioma growth modeling: Towards a fully personalized model?" *Cancers*, vol. 14, no. 10, 2022. [Online]. Available: https://www.mdpi.com/2072-6694/14/10/2530

[28] Y. Zhang, P. X. Liu, and W. Hou, "Modeling of glioma growth using modified reaction-diffusion equation on brain mr images," *Computer Methods and Programs in Biomedicine*, vol. 227, p. 107233, 2022. [Online]. Available: https://www.sciencedirect.com/science/article/pii/S0169260722006149

[29] P. K. Choudhary, "Some important contribution of modified crank-nicolson method for solving one dimensional parabolic equation," *International Journal of Emerging Technologies and Innovative Research*, vol. 6, no. 3, pp. 1144–1150, 2019. [Online]. Available: https://www.jetir.org/papers/JETIR1903K64.pdf

[30] O. B. Johnson and L. I. Oluwaseun, "Crank-nicolson and modified crank-nicolson scheme for one dimensional parabolic equation," *International Journal of Applied Mathematics and Theoretical Physics*, vol. 6, no. 3, pp. 35–40, 2020. [Online]. Available: http://dx.doi.org/10.11648/j.ijamtp.20200603.11

[31] S. C. Massey, R. C. Rockne, A. H. D. J. Gallaher, A. R. A. Anderson, P. Canoll, and K. R. Swanson, "Simulating pdgf-driven glioma growth and invasion in an anatomically accurate brain domain," *Bulletin of Mathematical Biology*, vol. 80, p. 1292–1309, 2018. [Online]. Available: https://link.springer.com/article/10.1007/s11538-017-0312-3

[32] L. J. Brooks, M. P. Clements, J. Burde, and et al, "The white matter is a pro-differentiative niche for glioblastoma," *Nature Communications*, vol. 12, no. 2184, 2021. [Online]. Available: https://www.nature.com/articles/s41467-021-22225-w

[33] F. Latini, M. Fahlström, A. Beháňová, I.-M. Sintorn, M. Hodik, K. Staxäng, and M. Ryttlefors, "The link between gliomas infiltration and white matter architecture investigated with electron microscopy and diffusion tensor imaging," *NeuroImage: Clinical*, vol. 31, p. 102735, 2021. [Online]. Available: https://www.sciencedirect.com/science/article/pii/S2213158221001790

[34] S. Tabassum, N. B. Rosli, and M. S. A. B. Mazalan, "Mathematical modeling of cancer growth process: A review," *Journal of Physics: Conference Series*, vol. 1366, no. 1, p. 012018, 2019. [Online]. Available: https://dx.doi.org/10.1088/1742-6596/1366/1/012018

[35] C. Vaghi, A. Rodallec, R. Fanciullino, J. Ciccolini, J. P. Mochel, M. Mastri, C. Poignard, J. M. L. Ebos, and S. Benzekry, "Population modeling of tumor growth curves and the reduced gompertz model improve prediction of the age of experimental tumors," *PLOS Computational Biology*, vol. 16, no. 2, pp. 1–24, 2020. [Online]. Available: https://doi.org/10.1371/journal.pcbi.1007178

[36] S. Udomchalermpat, S. Koonpraseart, and E.Kunnawuttipreechachan, "Dynamics of the generalized tumor-virotherapy model with time delay effect," *Engineering Letters*, vol. 28, no. 3, pp. 887–897, 2020.

[37] G. C. Manikis, K. Marias, D. M. J. Lambregts, K. Nikiforaki, M. M. van Heeswijk, F. C. H. Bakers, R. G. H. Beets-Tan, and N. Papanikolaou, "Diffusion weighted imaging in patients with rectal cancer: Comparison between gaussian and non-gaussian models," *PLOS ONE*, vol. 12, no. 9, pp. 1–15, 09 2017. [Online]. Available: https://doi.org/10.1371/journal.pone.0184197

[38] S. Subramanian, K. Scheufele, M. Mehl, and G. Biros, "Where did the tumor start? an inverse solver with sparse localization for tumor growth models," *Inverse Problems*, vol. 36, no. 4, p. 045006, 2020. [Online]. Available: https://dx.doi.org/10.1088/1361-6420/ab649c

[39] E. Akın, N. N. Pelen, I. U. Tiryaki, and F. Yalcin, "Parameter identification for gompertz and logistic dynamic equations," *PLOS ONE*, vol. 15, no. 4, pp. 1–21, 2020. [Online]. Available: https://doi.org/10.1371/journal.pone.0230582